Frequency-Related Effects in the Optimization of Coils for the Magnetic Stimulation of the Nervous System

Paolo Ravazzani*, Jarmo Ruohonen, Gabriella Tognola, Federica Anfosso, Marko Ollikainen, Risto J. Ilmoniemi, and Ferdinando Grandori

***Abstract*—Magnetic stimulation of the nervous system is a noninvasive technique with a large number of applications in neurological diagnosis, brain research, and, recently, therapy. New applications require engineering modifications in order to decrease power consumption and coil heating. This can be accomplished by optimized coils with minimized resistance. In this study the influence of some frequency-related effects (skin and proximity effect) on the coil resistance will be discussed, together with the role played by wire shape, wire section, and twisting effect. The results show that the coil resistance increases with frequency. As an example, for a 20-mm^2 circular wire section, the skin effect in the typical frequency range of magnetic stimulator devices (2–4 kHz) increases the coil resistance up to about 45% with respect to its dc value. Moreover, the influence of the frequency is lower for flat wire sections and reasonably small helix twist angle of the coil.**

***Index Terms*—Coil optimization, magnetic stimulation, proximity effect, skin effect.**

I. Introduction

THE human nervous system can be excited noninvasively using externally applied time-varying electromagnetic field pulses [2]. Magnetic stimulation (MS) is accomplished by driving an intense current pulse through a coil placed above the target nervous structures, which will induce a stimulating electric field. The poor linkage between the coil and the tissue limits the efficacy of MS: only $1/10^8$ of the magnetic energy in the coil is transmitted into the nervous tissues and, therefore, coil design is one of the key actions in order to improve and optimize MS. The required magnetic field of about 2 T is obtained by rapidly discharging a charged capacitor through the coil. An effective induced electric field can be obtained in the nervous tissues only when a current pulse with amplitude of up to 10 kA flows in the coil, and this, undoubtedly, represents the actual main engineering challenge of magnetic stimulation. Although certain types of pulse generation circuits allow the recovery of much of the energy as electrostatic energy in the discharge capacitor, part of the energy is dissipated in the coil resistance. The losses restrict the usefulness of MS since they increase the need of high-power electronics and coil cooling devices and limit both duration of operation and maximum achievable stimulus repetition rate when repetitive magnetic stimulation is performed.

While it is straightforward to calculate the resistance $R_{\rm dc}$ of an ideal coil at extremely low frequency, so far no detailed analysis has been performed to estimate the same quantities at higher frequency, in the following indicated as $R_{\rm ac}$. The coil resistance at the typical MS current frequencies from 2 to 4 kHz may be much greater than $R_{\rm dc}$, and this increase is mainly due to some frequency-related phenomena, such as the skin and proximity effects. The skin effect causes the current to concentrate near the wire surface, whereas the proximity effect causes an additional current redistribution in the coil windings due to the magnetic field from adjacent wires [9].

The aim of this study is the theoretical investigation of the influence of some frequency-related effects on the electric characteristics of nonideal air-cored coils, taking into account their application in magnetic stimulation. In particular, the study of the influence of the skin and proximity effect on the coil resistance and, consequently, on the dissipated energy, will be addressed considering both circular and rectangular wire sections. In order to make this paper more comprehensible, the theoretical approaches and the results are discussed in the main text, whereas the mathematical details are described in the appendices.

II. Theory

A. Skin Effect

Time-varying current flowing in a wire generates a changing magnetic field, which induces an eddy current in the wire itself. This phenomenon, known as the skin effect, causes the wire resistance to increase drastically with increasing frequency, because the current tends to concentrate near the surface of the wire [13], whereas the effect decreases only slightly the inductance [10]. Since the frequency content of the coil current in magnetic stimulation ranges usually from 2 to 4 kHz, the quasi-static (low-frequency) form of Maxwell's equations can be used.

Manuscript received July 25, 2001; revised December 25, 2001. This work coordinated within the framework of the European Research Project GUARD (Fifth Framework Programme, Quality of Life, under Contract QLK4-2001-00150, 2002–2005). This work supported by the Italian Consorzio Elettra 2000 in the framework of the Project ALERT (2001–2002) and by f the Finnish Technology Development Centre (TEKES). *Asterisk indicates corresponding author.*

*P. Ravazzani is with the Centro di Ingegneria Biomedica CNR, Piazza Leonardo da Vinci, 32 20133 Milan, Italy (e-mail: Paolo.Ravazzani@polimi.it).

J. Ruohonen and M. Ollikainen are with the Nexstim Ltd., FIN-00510 Helsinki, Finland.

G. Tognola, F. Anfosso, and F. Grandori are with the Centro di Ingegneria Biomedica CNR, 32 20133 Milan, Italy.

M. Ollikainen and R. J. Ilmoniemi are with the BioMag Laboratory, Medical Engineering Centre, Helsinki University Central Hospital, Helsinki, Finland.

Publisher Item Identifier S 0018-9294(02)03997-6.

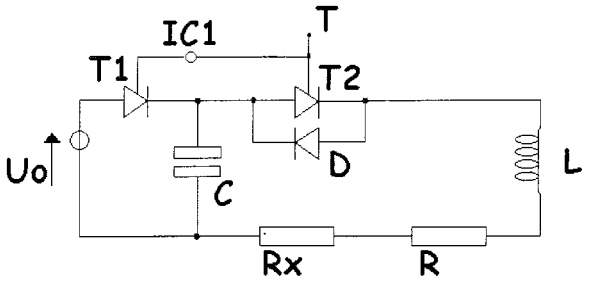

Fig. 1. Schematic illustration of the stimulator circuit. In commercial stimulators, typical values for power supply and components are $U_o = 2$ kV, $L = 15\ \mu$H, $C = 150\ \mu$F, $R = 50$ mΩ and $R_x = 10$ mΩ, thus obtaining a pulse duration of about 300 μs.

The mathematical approaches and the final formulations for the ratio between $R_{\rm ac}$ and $R_{\rm dc}$ for circular and rectangular wire section are discussed in Appendices I and II, respectively.

B. Proximity and Twisting Effect

When two or more adjacent conductors are carrying current, the current distribution in one conductor is affected by the magnetic flux produced by the adjacent conductors, as well as the magnetic flux produced by the current in the conductor itself. This effect is called the proximity effect and produces an increase of the wire resistance with the increase of the frequency. This increase is ordinarily greater than that one produced by the skin effect [4], [12], although it produces a similar influence on the current distribution, i.e., the current density is greatest in those parts of the conductor encircled by the smallest number of flux lines. For example, if a round wire is close to another wire carrying an equal current in the opposite direction, the fields will be additive between the two wires and opposed and canceled on the outsides. When the distance between wires is reduced the mutual cancellation increases. As a result, high-frequency currents are concentrated on the wire surfaces facing the other wire surface, where the field intensity is greatest, with little or no current on the outside surfaces where the field is low. However, this problem is more complicated than the study of the skin effect because the geometrical form of the magnetic field that causes the proximity effect changes with frequency. Moreover, when a coil winding spiraled to form a helix is considered, the influence of the proximity effect depends also by the angle of twist (see also Fig. 7 in Appendix IV) of each ring of the coil (twisting effect).

The mathematical approaches and the final formulations for the proximity effect in parallel wires and for the twisting effect are discussed in Appendices III and IV, respectively.

C. Dissipated Energy

The basic stimulator circuit consists of a capacitor C connected in series with the inductance L of the coil by a thyristor switch (Fig. 1). The total resistance $R_T = R_x + R$ in the circuit is due both to cables, capacitor, and thyristor (R_x) and coil (R, i.e., $R_{\rm dc}$ and $R_{\rm ac}$ at low and higher frequency, respectively). Closing the thyristor sets up a current pulse $I(t)$

$$I(t) = \frac{U_0 e^{-\alpha t} \sin \omega t}{\omega L} \tag{1}$$

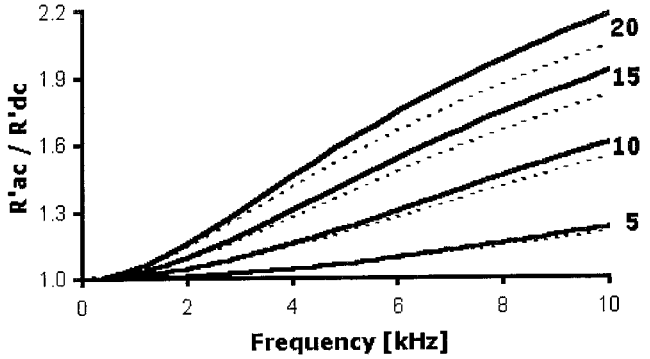

Fig. 2. Influence of the skin effect on the coil resistance per unit length at high-frequency $R'_{\rm ac}$ of a copper coil as a function of the frequency of the coil current. The effect is shown as the ratio $R'_{\rm ac}/R'_{\rm dc}$, where $R'_{\rm dc}$ is the coil resistance per unit length. The ratio is computed for different wire sections and for circular (see Appendix I) and rectangular (see Appendix II) wire shape. The solid and dashed lines represent circular and rectangular wire shape, respectively. In each case, the section (expressed in millimeters squared) is shown on the right of each corresponding couple (continuous and dotted) of curves. In this case, for the rectangular wire shape, the ratio between the height h and the width w of the wire section was set to one, thus obtaining a square wire shape. Here and in the following Figures, the computation was performed by the software package MATLAB.

where $\alpha = R_T/2L$, $\omega^2 = (LC)^{-1} - \alpha^2$ and U_0 is the capacitor's charging voltage. The diode D connected anti-parallel with the thyristor is included when a biphasic wave shape of the current should be obtained, that allows the recovery of some of the magnetic energy in the coil as electrostatic energy of the capacitor.

Energy is dissipated as Joule heating in the coil, cables, and electronics components. The energy dissipated can be estimated by the following expression:

$$W_J = R_T \int_0^{\Delta t} I^2(t) dt \tag{2}$$

where Δt is the pulse duration.

The integral in the equation above can be computed as [11]

$$\int_0^{\Delta t} I^2(t) dt = \frac{U_0^2}{4L^2\omega^2(\alpha^2+\omega^2)} \left[e^{-2\alpha\Delta t}(\alpha \cos 2\omega\Delta t - \omega \sin 2\omega\Delta t - (\alpha^2+\omega^2)\alpha^{-1}) + \omega^2\alpha^{-1} \right]. \tag{3}$$

The energy dissipated during one pulse inducing a given electric field at the target can be used as figure of merit for the efficacy of the stimulator.

III. Results

A. Skin Effect

Fig. 2 shows the influence of the skin effect on a coil with different wire sections and wire shapes (circular and squared wire). The results are given as ratio between $R'_{\rm ac}$ and $R'_{\rm dc}$ (i.e., $R_{\rm ac}$ and $R_{\rm dc}$ per unit length) versus frequency of the current flowing in the coil. Disregarding the wire shape, the skin effect increases the coil resistance, in particular for larger wire sections. At the maximum considered section of 20 mm^2, the increase of the $R'_{\rm ac}$ over $R'_{\rm dc}$, ranges from 16% at 2 kHz to 45% at 4 kHz for circular and from 14% to 41% for square wire sections. On the other hand, at the minimum wire section of 5 mm^2,

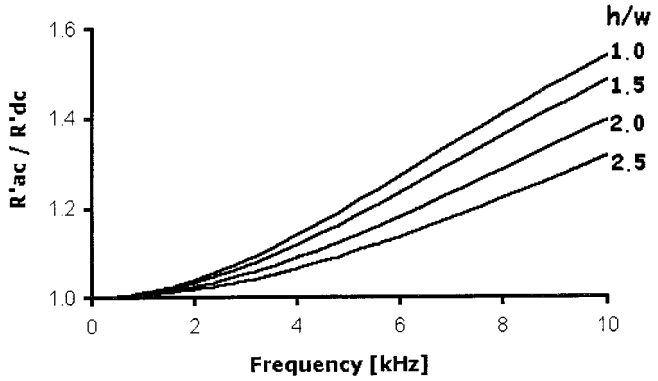

Fig. 3. Ratio R'_{ac}/R'_{dc} over frequency for rectangular wire section (see Appendix II). The ratio is computed for different height h and width w of the wire section. In all cases, the section is set to 10 mm^2.

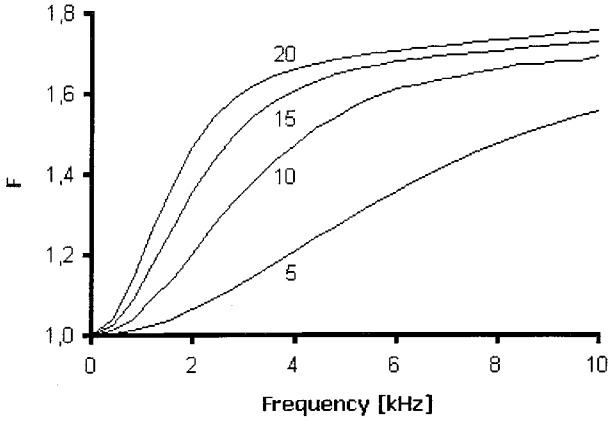

Fig. 4. Proximity factor F, obtained by normalizing R'_{ac} with respect to R'_{ac} of an isolated conductor, i.e., $F = R'_{ac}/R'_{ac(isolated)}$ (see Appendix III), versus the current frequency in a helix-shaped coil. The effect of different circular sections (expressed in mm^2 on top of each curve) is also shown. The angle of twist β is set to 90°.

R'_{ac} increases with respect to R'_{dc} from about 2.4% (at 2 kHz) to 5.5% (at 4 kHz), both for circular and squared wire.

Fig. 3 illustrates the change in R'_{ac}/R'_{dc} versus frequency for rectangular wire with different height h and width w ratio and identical wire section of 10 mm^2. The resistance ratio is greatest for squared wire, i.e., h/w equal to one (the increase of R_{ac} over R_{dc} ranges from 4% to 15% at 2 and 4 kHz, respectively), and decreases as the wire becomes flat, i.e., h much greater than w. For example, for $h/w = 2.5$, the increase of R_{ac} over R_{dc} is of 2% and 6.4%, at 2 and 4 kHz, respectively.

B. Proximity and Twisting Effect

Fig. 4 shows the proximity effect as proximity factor F, obtained by normalizing R'_{ac} with respect to R'_{ac} of an isolated conductor, i.e., $F = R'_{ac}/R'_{ac(isolated)}$. The results are given for different wire sections versus coil frequency, for a helix-shaped copper coil with given twist angle β of 90°. Fig. 5 shows F versus frequency for helices with different β, with given section of 10 mm^2. Considering the change in wire section, F shows an abrupt change versus frequency. All curves show a rapid increase up to 4 kHz and then saturation, with a reduction in the slope of the curves with the decrease of the section. However, in the typical current frequency range of magnetic stimulation

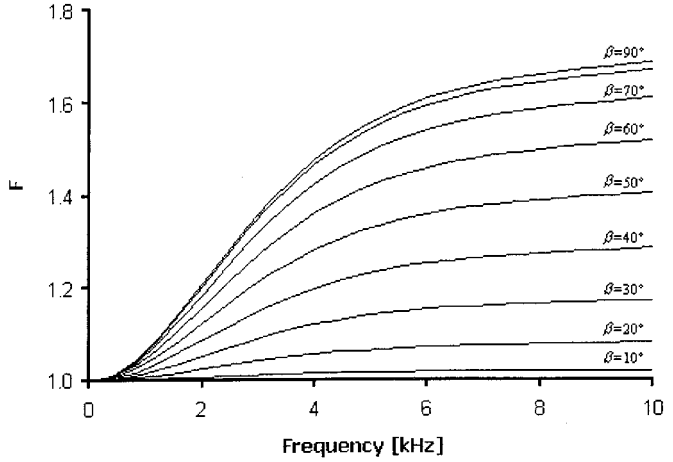

Fig. 5. Proximity factor F versus the current frequency in a helix-shaped coil (see Appendix IV). The effect of different angle of twist β (on top of each curve) is also shown. The circular section is set to 10 mm^2.

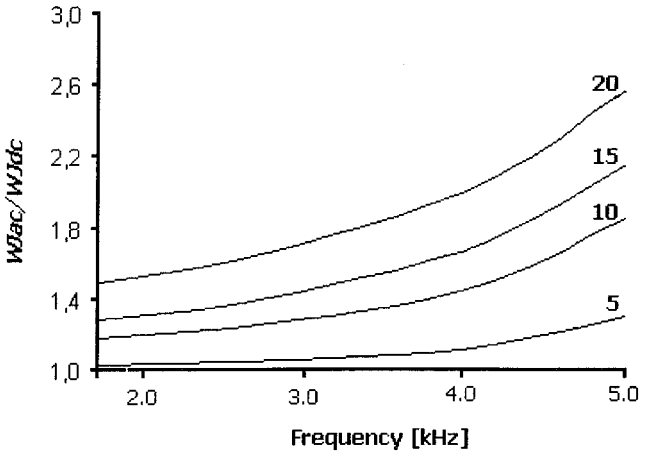

Fig. 6. Ratio between the dissipated energy [computed on the basis of (2)] at high-frequency (W_{Jac}) computed taking into account skin and proximity effect and its value at low-frequency (W_{Jdc}) versus the current frequency, changing the wire sections (expressed in millimeters squared). The inductance of the 5-cm radius circular coil is of 32 μH in all cases.

devices, for a wire section of 5 mm^2, F increases of about 6.3% and 21.3%, at 2 and 4 kHz, respectively, with a relative increase of about 14.1%, whereas, for a wire section of 20 mm^2, F increases of about the 48.8% and 67.3%, at 2 and 4 kHz, respectively, with a relative increase of about 12.9%.

As to the twisting effect (Fig. 5), for a given section of 10 mm^2, the proximity factor is greatest for tightly packed helices. For a twist angle β of 45°, the increase is of about 8.6% and 20%, at 2 and 4 kHz, respectively (relative increase of about 10.4%), whereas when the helix becomes loose and long ($\beta =$ 10°), F can be considered approximately equal to unity at all frequencies.

C. Dissipated Energy

Taking into account the skin and proximity effect, the dissipated energy W_{Jac} can be computed by (2) and compared with the dissipated energy calculated with the coil resistance at low-frequency (W_{Jdc}). Fig. 6 represents the ratio W_{Jac}/W_{Jdc} versus frequency of the current flowing in the coil, for a circular wire, considering different wire sections. For a wire section of

20 mm^2, W_{Jac} increases of about 53% and 101% with respect W_{Jdc}, at 2 and 4 kHz, respectively. This effect reduces as the wire section decreases. For a 5-mm^2-wire section, the increase of W_{Jac} with respect W_{Jdc} is of about 3.4% and 9.1%, at 2 and 4 kHz, respectively.

IV. Discussion

Magnetic stimulation of the nervous system is a noninvasive technique with a large number of applications in neurological diagnosis, brain research, and, recently, in therapy. The applications of magnetic stimulation are becoming increasingly sophisticated, and users demand stimulators with less coil warming, with better capabilities of focusing the stimulating fields in small regions and capable of delivering more rapid trains of stimuli for repetitive transcranial stimulation. Moreover, therapeutic use of magnetic stimulation appears an exciting and promising application in the near future, being particularly true for functional and rehabilitative stimulation [14]. In that sense, recently, the application of magnetic stimulation to functional magnetic stimulation (FMS) may provide a fascinating option and additional tool to the conventional functional electric stimulation. Several FMS experiments have already been described in literature. Lin *et al.* assessed the possibility of FMS to help bladder emptying and training in individuals with spinal cord injury [16]. Craggs *et al.* discussed the possibility to use FMS of the phrenic nerve for respiratory muscle function [17]. Sheriff *et al.* reported that FMS over the sacrum could profoundly suppress detrusor hyper-reflexia resulting from spinal cord injury [18]. However, to enable the use of magnetic stimulation as an alternative of electrical stimulation for functional or rehabilitation purposes, it is crucial to optimize the available stimulating devices, and the key to optimization is coil design [11], [14], [19].

Few papers in literature address coil optimization. In one study, 8-shaped and 4-leaf coils with various angles between the wings, as to better fit the shape of the tissue surface, were analyzed along with square and circular loop shapes [20]. The effect of the size of the circular coil was analyzed by, e.g., Ruohonen *et al.* [21] and the degree to which the field can be concentrated by Ravazzani *et al.* [22]. These studies considered the relationship between the amplitude of the driving current and the magnitude of the induced field, which, however, is not a measure of the efficacy of the coil or the stimulator. In context of repetitive brain stimulation, the analysis has been extended to minimize the stimulator's power consumption, coil heating and the peak magnetic energy [11]. These last results do not apply directly for magnetic stimulation, since the activating mechanisms in brain and peripheral stimulation are thought to be different. For the stimulation of curved axons or near terminations, such as in nerve root stimulation, coils similar to those used in brain stimulation may be useful.

Coil design depends greatly on the application and there is no globally optimal solution [11]. Ruohonen *et al.* [14] analyzed where the copper loops inside the coil should be placed to achieve the required electric field gradient along the nerve with the minimum driving energy in the coil. For this purpose, they cast the coil geometry in terms of six parameters that define the size, shape, type, and winding profile of the coil. One prominent result of analyzing how changes in the geometry factors affect the driving energy was that single and 8-shaped coils are much less effective than 4-leaf coils. Another conclusion was that D-shaped wings are better over elliptic or circular wings and that the winding profile should preferably be flat with many concentric layers. The optimum outer wing diameter was found to be 40–50 mm. Although smaller coils have been suggested on the basis of field modeling, our results indicate that the reduced inductance of small coils is not enough to compensate for the greater driving current.

In general terms, in order to optimize the device, no single parameter adequately characterizes the stimulator. The goodness of this kind of apparatus is a mixture of various factors, among which the following can only be considered essential elements for its design: 1) adequate energy transfer (current flow $\times$ pulse duration) to depolarize neurons; 2) restricted flow outside the area of interest (high focusing); 3) acceptable allowed repetition rate; 4) patient and operator safety; 5) tolerable heat build-up; and 6) acceptable weight, cost, reliability, convenience, and availability.

This paper, ultimately, addresses the study of the power consumption of magnetic stimulators, substantially influenced by two main factors, the efficacy of the stimulator, i.e., the power dissipation in the coil and cables during the stimulus delivery phase and the efficacy of the coil in transmitting energy into the brain. The latter is affected by the coil winding [11], whereas the power dissipation can be decreased by optimizing the shape and size of the coil wire in order to minimize the coil resistance that depends greatly on frequency-related effects such as the skin and proximity effect and, hence, on the frequency of the current in the coil. These phenomena increase the R_{ac} with respect to R_{dc} with the increase of both frequency and wire section. Their influence depends also by the shape of the wire cross section, affecting more circular than square and rectangular wire cross section. Considering the skin effect, at 4 kHz (at the top end of the typical range of the coil current frequency in magnetic stimulation devices), with the smallest wire section (5 mm^2), the increase of R_{ac} over R_{dc} is approximately equal for circular and square wire shape, whereas for larger wire sections (15–20 mm^2), R_{ac} shows a larger increase for circular than for square wire shape. This is also confirmed for rectangular wire shape, with a decrease of the influence of the skin effect as the wire shape becomes flat.

Similarly, the influence of the proximity effect on the coil resistance is greater for larger wire sections than for smaller ones. Moreover, in a helix-shaped coil, the coil resistance is lower for long (lower twist angle β) and higher for short helices (higher twist angle β). As a consequence, the change in coil resistance versus frequency produces a dramatic change in the dissipated energy of the device and this effect is greater for larger wire section.

The influence of the frequency-related effects investigated here can be discussed considering some typical characteristic of actual clinical and research magnetic stimulator devices, i.e., coil-current frequency content between 2 and 4 kHz, wire section of about 5 to 10 mm^2, circular or rectangular wire shape [2], [11], [14], [15]. As an example, the increase of R_{ac} over

$R_{\rm dc}$, for circular wire shapes and coil-current frequency of 3 kHz is of about 10.8% considering the skin effect (Fig. 2), of about 15.1%, considering the proximity effect (Fig. 4), with an increase in dissipated energy of about 27.4% (Fig. 6). The use of a rectangular wire shape, with a width/length ratio of 2.0 and a cross section of 10 mm^2, produces an increase of $R_{\rm ac}$ over $R_{\rm dc}$ of about 5.1% (Fig. 3).

As a last remark, one should note that the change in coil resistance due to the frequency intrinsically produces a change of the electric circuit of the stimulator, yielding a consequent change of the frequency of the current. This phenomenon is not taken under consideration in the approach presented here, but, although, actually in the frequency range from 2 to 4 kHz it can be considered negligible, this issue should be better investigated in next studies.

In summary, the results presented here show that the changes in coil electric parameters due to the frequency-related effects discussed here cannot be neglected in designing magnetic stimulation devices. As to the coil optimization, this study suggests that, in order to reduce the influence of these effects, the use of wire with small section, flat shape and with a reasonably small helix twist angle is advisable.

Appendix I
Skin Effect in Circular Wire Section

The current-density $\mathbf{J}$ in a circular conductor can be most conveniently computed using the cylindrical coordinates r, ϕ and z. The boundary conditions imply that the r and z components of the magnetic field $\mathbf{H}$ vanish ($H_z = H_r = 0$), and that only the z component of $\mathbf{J}$ is not identically zero. Because of the cylindrical symmetry, both derivatives of $\mathbf{H}$ and $\mathbf{J}$ with respect to ϕ are always equal to zero.

By Maxwell equations in cylindrical coordinates and by the Faraday Induction Law one can obtain the following Bessel differential equation of the first kind and order zero:

$$\frac{d^2J_z}{dr^2} + \frac{dJ_z}{rdr} = j\omega\sigma\mu J_z \tag{AI-1}$$

where $j = \sqrt{-1}$, μ is the magnetic permeability ($4\pi \times 10^{-7}$ H/m for air as well as for copper), σ is the electric conductivity (5.8×10^7 $1/\Omega$m for copper), and r is the distance between a point inside the cross section and the center of the cross section itself. These latter two quantities are independent from the frequency. The solution of (AI-1) is:

$$J_z = AI_0\left(j^{(1/2)}kr\right) + BK_0\left(j^{(1/2)}kr\right) \tag{AI-2}$$

where $I_0\left(j^{(1/2)}kr\right)$ is the modified Bessel function of first kind and order zero, $K_0\left(j^{(1/2)}kr\right)$ is the modified Bessel function of second kind and order zero and $k^2 = \omega\sigma\mu$. A and B can be determined by the boundary conditions. In order to avoid a infinite current along the conductor axis ($r = 0$), B should be zero. Taking into account that

$$I_0\left(j^{(1/2)}kr\right) = J_0\left(j^{(3/2)}kr\right) \tag{AI-3}$$

where $J_0\left(j^{(3/2)}kr\right)$ is the Bessel function of first kind and order zero; Bessel functions with complex argument $j^{(3/2)}kr$ are generally expressed by [8]

$$J_n\left(j^{(3/2)}x\right) = \mathrm{ber}_n(x) + j\mathrm{bei}_n(x) \tag{AI-4}$$

where ber_n and bei_n stands for the Kelvin functions of order n. Their general expressions are

$$\mathrm{ber}_n(x) = \sum_{m=0}^{\infty} \frac{(-1)^m\left(\frac{x}{2}\right)^{n+2m}}{m!\Gamma(n+m+1)} \cos\frac{3}{4}(n+2m)\pi \tag{AI-5}$$

$$\mathrm{bei}_n(x) = \sum_{m=0}^{\infty} \frac{(-1)^m\left(\frac{x}{2}\right)^{n+2m}}{m!\Gamma(n+m+1)} \sin\frac{3}{4}(n+2m)\pi. \tag{AI-6}$$

$\Gamma(n+1)$ is the Gamma function. For all values of x, these series are convergent [3]. The constant A is then easily calculated by equating the surface integral of current density to the total current I over the cross section with radius r_w

$$\begin{aligned} I &= \int_s J_z ds = 2\pi A \int_0^{r_w} rJ_0\left(j^{(3/2)}kr\right)dr \\ &= \frac{2\pi}{j^{(3/2)}k} Ar_w J_1\left(j^{(3/2)}kr_w\right). \end{aligned} \tag{AI-7}$$

This can be obtained on the base of the classical formulation

$$\int_0^a z^{-v}J_{v+1}(hz)dz = \frac{a}{h}J_v(ha). \tag{AI-8}$$

Now the current density over the conductor cross section can be computed as

$$J_z = I\frac{j^{(3/2)}k}{2\pi r_w J_1\left(j^{(3/2)}kr_w\right)} J_0(j^{(3/2)}kr) \tag{AI-9}$$

where r_w is the wire radius.

The resistance $R_{\rm ac}$, taking into account the skin effect, can be determined, from the dissipated power per unit length of the wire P' in W/m, as [5], [6], [8]

$$\begin{aligned} P' &= \frac{\pi}{\sigma}\int_0^{r_w} J_z(r)J_z^*(r)rdr \\ &= \frac{I_{\rm peak}^2 k}{\pi\sigma\left[2r_w J_1\left(j^{(1/2)}kr_w\right)\right]^2}\int_0^{r_w} I_0\left(j^{(1/2)}kr\right) \\ &\quad \times I_0\left(j^{-(1/2)}kr\right)rdr \end{aligned} \tag{AI-10}$$

where $J_z^*(r)$ is the complex conjugate of $J_z(r)$ and $I_{\rm peak}$ is the amplitude of the coil current I. The right-hand-side integral can be evaluated using Lommel integrals [8]

$$P' = \frac{I^2 k}{2\pi r_w \sigma}\frac{M_0(kr_w)}{M_1(kr_w)}\sin\left(\theta_1 - \theta_0 - \frac{\pi}{4}\right) \tag{AI-11}$$

where M_0, M_1, θ_0, and θ_1 are

$$M_v(kr_w) = \sqrt{\mathrm{ber}_v^2(kr_w) + \mathrm{bei}_v^2(kr_w)} \tag{AI-12}$$

$$\theta_v(kr_w) = \tan^{-1}\left(\frac{\mathrm{bei}_v(kr_w)}{\mathrm{ber}_v(kr_w)}\right) \tag{AI-13}$$

where v is the order of the Bessel functions. It can be demonstrated that the Kelvin functions converge in the range of values assumed by kr_w [8].

Now, one should take into account that

$$P' = R'_{\mathrm{ac}} I^2_{\mathrm{rms}} \tag{AI-14}$$

where I_{rms} is the root-mean-square value (rms) of the coil current I and, as stated before, P' and R'_{ac} are, respectively, the dissipated power and the resistance of the coil at high-frequency per unit length of the wire. Hence, one can easily compute R'_{ac} by combining (AI-11) and (AI-14)

$$R'_{\mathrm{ac}} = \frac{k}{2\pi r_w \sigma}\frac{M_0(kr_w)}{M_1(kr_w)}\sin\left(\theta_1 - \theta_0 - \frac{\pi}{4}\right). \tag{AI-15}$$

The resistance of the coil at low frequency per unit length (R'_{dc}) can be simply estimated by

$$R'_{\mathrm{dc}} = \frac{1}{\sigma S} \tag{AI-16}$$

where S is the cross-sectional area of the wire, thus obtaining

$$\frac{R'_{\mathrm{ac}}}{R'_{\mathrm{dc}}} = \frac{Sk}{2\pi r_w}\frac{M_0(kr_w)}{M_1(kr_w)}\sin\left(\theta_1 - \theta_0 - \frac{\pi}{4}\right). \tag{AI-17}$$

Appendix II
Skin Effect in Rectangular Wire Section

Within a certain approximation, the resistance and reactance of a rectangular conductor (cross-sectional area $S_r = 2b \times 2h$) can be quite accurately calculated as a two-dimensional (2-D) problem [5], [23]. In this case, the current density is given by the differential equation

$$\frac{\partial^2 J}{\partial x^2} + \frac{\partial^2 J}{\partial y^2} = l^2 J \tag{AII-1}$$

where $l^2 = j\omega\sigma\mu$. This partial differential equation can be converted into an ordinary differential equation through Fourier Transform [1]. Assuming that the magnetic flux does not pass through the surface of this conductor into an adjacent conductor, the lines of force in the thin surface layer can be considered as following the boundaries of its cross section. Then, the current-density J over this thin surface layer will be the same in all the rectangular section $x = \pm b$, $y = \pm h$ and can be expressed, considering a sinusoidal waveform, in the form

$$J = J_0 \sin(\omega t + \varphi). \tag{AII-2}$$

If this conductor carries a current I of rms. (root mean square) value I_{rms} and the linear current density at low frequency (i.e., without considering the skin effect) is denoted by J_{dc} as the amplitude of the current density at low frequency, i.e., without considering the skin effect, then

$$4bhJ_{\mathrm{dc}}\sin(\omega t) = \sqrt{2} I_{\mathrm{rms}} \sin(\omega t) = \int_{S_r} J\,dx\,dy. \tag{AII-3}$$

Taking into account the surface conditions ($x = \pm b$ and $y = \pm h$) given by (AII-2), the solution of the (AII-1) is given by the series

$$J = \frac{4}{\pi} J_0 \sum_{n=1,3,5,\ldots}^{\infty} \frac{j^{n-1}}{n}\left[\frac{\cosh\sqrt{\left(\frac{l^2+n^2\pi^2}{4h^2}\right)}\,x}{\cosh\sqrt{\left(\frac{l^2+n^2\pi^2}{4h^2}\right)}\,b}\cos\frac{n\pi}{2h}y + \frac{\cosh\sqrt{\left(\frac{l^2+n^2\pi^2}{4b^2}\right)}\,y}{\cosh\sqrt{\left(\frac{l^2+n^2\pi^2}{4b^2}\right)}\,h}\cos\frac{n\pi}{2b}x\right] \times \sin(\omega t + \varphi). \tag{AII-4}$$

Hence, in combination with (AII-3) one can obtain

$$4bhJ_{\mathrm{dc}}\sin(\omega t) = \frac{32}{\pi^2} J_0 bh \sum_{n=1,3,5,\ldots}^{\infty} \frac{1}{n^2}\left[\frac{\tanh\sqrt{\left(\frac{l^2+n^2\pi^2}{4h^2}\right)}\,b}{\sqrt{\left(\frac{l^2+n^2\pi^2}{4h^2}\right)}\,b} + \frac{\tanh\sqrt{\left(\frac{l^2+n^2\pi^2}{4b^2}\right)}\,h}{\sqrt{\left(\frac{l^2+n^2\pi^2}{4b^2}\right)}\,h}\right] \times \sin(\omega t + \varphi). \tag{AII-5}$$

The complex values under the radical sign can be expressed by the components

$$\left(l^2 + \frac{n^2\pi^2}{4h^2}\right)b^2 = (\alpha_n + j\beta_n)^2$$
$$\left(l^2 + \frac{n^2\pi^2}{4b^2}\right)h^2 = (\alpha_m + j\beta_m)^2 \tag{AII-6}$$

from which follow the expressions:

$$\alpha_n = \frac{n\pi}{2\sqrt{2}}\frac{b}{h}\sqrt{\left\{\sqrt{\left[\left(\frac{\omega\sigma\mu h^2}{n^2\pi^2}\right)^2 + 1\right]} + 1\right\}}$$
$$\alpha_m = \frac{n\pi}{2\sqrt{2}}\frac{h}{b}\sqrt{\left\{\sqrt{\left[\left(\frac{\omega\sigma\mu b^2}{n^2\pi^2}\right)^2 + 1\right]} + 1\right\}}$$
$$\beta_n = \frac{n\pi}{2\sqrt{2}}\frac{b}{h}\sqrt{\left\{\sqrt{\left[\left(\frac{\omega\sigma\mu h^2}{n^2\pi^2}\right)^2 + 1\right]} - 1\right\}}$$
$$\beta_m = \frac{n\pi}{2\sqrt{2}}\frac{h}{b}\sqrt{\left\{\sqrt{\left[\left(\frac{\omega\sigma\mu b^2}{n^2\pi^2}\right)^2 + 1\right]} - 1\right\}}. \tag{AII-7}$$

Then, one will be able to write in (AII-3) simply

$$\frac{\tanh(\alpha_n + j\beta_n)}{\alpha_n + j\beta_n} = A_n - jB_n \tag{AII-8}$$
$$\frac{\tanh(\alpha_m + j\beta_m)}{\alpha_m + j\beta_m} = A_m - jB_m. \tag{AII-9}$$

By suitable arrangement one can obtain the general equations for A and B

$$A = \frac{\alpha\sinh 2\alpha + \beta\sin 2\beta}{(\alpha^2+\beta^2)(\cosh 2\alpha + \cos 2\beta)} \tag{AII-10}$$

$$B = \frac{\beta \sinh 2\alpha - \alpha \sin 2\beta}{(\alpha^2+\beta^2)(\cosh 2\alpha + \cos 2\beta)}. \quad \text{(AII-11)}$$

Then, the sum of the series in (AII-5) can also be simplified

$$\sum_{n=1,3,5,\ldots}^{\infty} \frac{1}{n^2}(A_n + A_m) = A_N + A_M$$
$$\sum_{n=1,3,5,\ldots}^{\infty} \frac{1}{n^2}(B_n + B_m) = B_N + B_M. \quad \text{(AII-12)}$$

Equation (AII-5) assumes, after all conversions, the form

$$4J_{\rm dc}\sin\omega t = \frac{32}{\pi^2}J_0[(A_N + A_M)\sin(\omega t + \varphi) - (B_N + B_M)\cos(\omega t + \varphi)]. \quad \text{(AII-13)}$$

For $\omega t = 0$, the phase angle follows from the equation:

$$\tan\varphi = \frac{B_N + B_M}{A_N + A_M} \quad \text{(AII-14)}$$

and for $\omega t = \pi/2$, one can obtain

$$\frac{J_0\cos\varphi}{J_{\rm dc}} = \frac{\pi^2}{8}\frac{A_N + A_M}{(A_N + A_M)^2 + (B_N + B_M)^2}. \quad \text{(AII-15)}$$

From the last two equations the expression for the resistance (and reactance) follow without the necessity to solve the expressions for J_0 and φ. At the time $\omega t = \pi/2$ the voltage drop in the conductor disregarding or not the skin effect is equal to the exciting voltage. From (AII-2) one can obtain on the surface of the conductor the drop

$$\frac{J_s}{\sigma} = \frac{J_0\cos\varphi}{\sigma}. \quad \text{(AII-16)}$$

Equating this drop to that of the linear current density in the changed conductivity

$$\frac{\sqrt{2}I}{4bh\sigma_{\rm ac}} = \frac{J_{\rm dc}}{\sigma_{\rm ac}} \quad \text{(AII-17)}$$

where $\sigma_{\rm ac}$ is the apparently reduced conductivity due to the skin effect. Then the ratio expressing the increase of resistance is then given by

$$\frac{R'_{\rm ac}}{R'_{\rm dc}} = \frac{\sigma}{\sigma_{\rm ac}} = \frac{J_0\cos\varphi}{J_{\rm dc}} = \frac{\pi^2}{8}\frac{A_N + A_M}{(A_N + A_M)^2 + (B_N + B_M)^2}. \quad \text{(AII-18)}$$

Appendix III
Proximity Effect in Parallel Wires

A finite round wire that carries a current I is located close to an infinitesimal wire carrying a current I_1 can be considered as a simple example of proximity effect in wires [7]. If J varies harmonically with frequency the equation that describes the current distribution becomes [9]

$$\frac{\partial^2 J}{\partial r^2} + \frac{1}{r}\frac{\partial J}{\partial r} + \frac{1}{r^2}\frac{\partial^2 J}{\partial \theta^2} = \mu\sigma\frac{\partial J}{\partial t} = 2\pi f\mu\sigma J. \quad \text{(AIII-1)}$$

If r and θ are the polar coordinates of a point inside the wire, r_w is the radius of the wire, s is the distance from the center of the wire to the infinitesimal wire, n is an integer, and k is equal to $2\pi f\mu\sigma$, the solution of this equation becomes [3]

$$J(r,\theta) = \frac{Ij^{(3/2)}k}{2\pi r_w}\frac{J_0\left(j^{(3/2)}kr\right)}{J_1\left(j^{(3/2)}kr_w\right)} + \frac{Ij^{(3/2)}k}{2\pi r_w}\sum_{n=0}^{\infty}\frac{r_w^n}{s^n}\frac{J_n\left(j^{(3/2)}kr\right)}{J_{n-1}\left(j^{(3/2)}kr_w\right)}\cos(n\theta) \quad \text{(AIII-2)}$$

where J_n is a Bessel function of the first kind and order n.

An expression for the magnetic field at any point of the surface of the wire was proposed by Dwight [3], who used the Poynting theorem to find the resistance loss in the wire. When $I_1 = I$ the value of the resistance ratio can be computed by (AIII-3), shown at the bottom of the page.

The first part of this equation is the expression for an isolated wire, and the second part gives the increase due to the proximity effect.

In order to quantify the changes in $R'_{\rm ac}$, the proximity factor F is introduced as the ratio between $R'_{\rm ac}$ and $R'_{\rm ac}$ computed for an isolated conductor

$$F = \frac{R'_{\rm ac}}{R'_{\rm ac(isolated)}}. \quad \text{(AIII-4)}$$

Appendix IV
Twisting Effect

Typically, the coil resistance is computed by the one-dimensional approximation, based on converting its circular conductors into a single flat sheet of the same thickness [6].

An increased accuracy can be yielded applying a 2-D model to compute $R_{\rm ac}$. The coiled winding is assumed to be spiraled to form a helix. Its radius is r_c, the wavelength or pitch is λ, as shown in Fig. 7, where the angle of twist β is also shown.

An increase in $R_{\rm ac}$ is attributed to a longitudinal magnetic field, H_z, inside the helix, which is proportional to $\sin\beta$. The actual current resistance of the twisted conductor can be obtained by computing the power dissipation per unit length, as done before for the straight wire. It is a sort of effect of superposition: first consider the skin effect, which induces a current-density J_z. The power dissipated per unit length due to the skin effect can be calculated as

$$P' = \frac{I^2 k}{2\pi\sigma 2r_w}\frac{M_0(kr_w)}{M_1(kr_w)}\sin\left(\theta_1 - \theta_0 - \frac{\pi}{4}\right). \quad \text{(AIV-1)}$$

$$\frac{R'_{\rm ac}}{R'_{\rm dc}} = \frac{k}{2\pi r_w\sigma}\left(\frac{M_0(kr_w)}{M_1(kr_w)}\sin\left(\theta_1 - \theta_0 - \frac{\pi}{4}\right) + 2\sum_{n=1}^{\infty}\frac{r_w^{2n}}{s^{2n}}\frac{(\mathrm{ber}_n(kr_w)\mathrm{bei}_{n+1}(kr_w) - \mathrm{ber}_{n+1}(kr_w)\mathrm{bei}_n(kr_w))}{(\mathrm{ber}_{n-1}^2(kr_w) - \mathrm{bei}_{n-1}^2(kr_w))}\right). \quad \text{(AIII-3)}$$

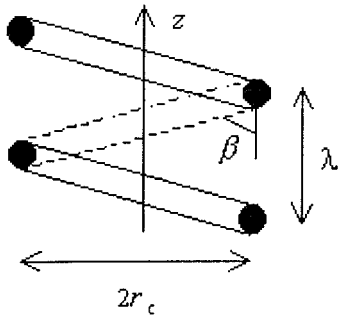

Fig. 7. Schematic representation of a helix-shaped coil: r_c is the coil radius, λ is the wavelength or pitch, whereas β is the angle of twist.

The proximity effect induces a current-density component parallel to the wire surface, J_Φ, which causes a heat loss in the ring given by

$$dP' = \frac{1}{2} J_\phi^2 dr^2 \left(\frac{2\pi r}{\gamma dr}\right) = \frac{I^2 k^2}{2\pi r_w^2 2\sigma} \sin^2\beta \left[\frac{J_1\left(j^{(3/2)}kr\right)}{J_0\left(j^{(3/2)}kr_w\right)}\right]^2. \quad \text{(AIV-2)}$$

where $J_n()$, as said before, are the Bessel functions of the first kind and order n. The total loss per unit length [W/m] can then be computed by means of the Lommel integral

$$P' = \frac{I^2}{2} R = \frac{1}{2} \frac{I^2 k}{2\pi r_w \sigma} \sin^2\beta \frac{M_1(kr_w)}{M_0(kr_w)} \cos\left(\theta_1 - \theta_0 - \frac{\pi}{4}\right). \quad \text{(AIV-3)}$$

Then, the total resistance of the twisted wire (R'_{ac}) per unit length (Ω/m) can be obtained as

$$R'_{\text{ac}} = \frac{k}{2\pi r_w \sigma} \left\{ \frac{M_0(kr_w)}{M_1(kr_w)} \sin\left(\theta_1 - \theta_0 - \frac{\pi}{4}\right) + \sin^2\beta \frac{M_1(kr_w)}{M_0(kr_w)} \cos\left(\theta_1 - \theta_0 - \frac{\pi}{4}\right) \right\} \quad \text{(AIV-4)}$$

Also in this case, as for the discussion of the proximity effect, in order to quantify the changes in R'_{ac}, the proximity factor F is introduced.

REFERENCES

[1] G. Arfken, *Mathematical Methods for Physicists*. New York: Academic, 1985.

[2] S. Chokroverty, *Magnetic Stimulation in Neurophysiology*. London, U.K.: Butterworth, 1990.

[3] H. B. Dwight, *Electrical Coils and Conductors*. New York: McGraw-Hill, 1945.

[4] D. I. Hoult and P. Lauterbur, "The sensitivity of the zeugmatographic experiment involving human samples," *J. Magn. Reson.*, vol. 34, 1979.

[5] J. Lammeraner and M. Stafl, *Eddy Currents*. London, U.K.: Ilife Books LTD, 1966.

[6] A. W. Lofti, P. M. Gradzki, and F. C. Lee, "Proximity effects in coils for high frequency power applications," *IEEE Trans Magn.*, vol. 28, pp. 2169–2171, Sept. 1992.

[7] C. Manneback, "An integral equation of skin effect in parallel conductors," *J. Math. Phys.*, April 1922.

[8] N. W. McLachlan, *Bessel Functions for Engineers*. Oxford, U.K.: Oxford Univ. Press, 1934.

[9] E. B. Moullin, *The Principles of Electromagnetism*. Oxford, U.K.: Claredon, 1955.

[10] ——, *The Theory and Practice of Radio Frequency Measurements*. London, U.K.: Griffin, 1931.

[11] J. Ruohonen, J. Virtanen, and R. J. Ilmoniemi, "Coil optimization for magnetic brain stimulation," *Ann. Biomed. Eng.*, vol. 25, pp. 840–849, 1997.

[12] F. Terman, *Electronic and Radio Engineering*. New York: McGraw-Hill, 1955.

[13] ——, *Radio Engineers' Handbook*. New York: McGraw-Hill, 1943.

[14] J. Ruohonen, P. Ravazzani, and F. Grandori, "Functional magnetic stimulation: Theory and coil optimization," *Bioelectrochem. Bioenergetics*, vol. 47, pp. 213–219, 1998.

[15] W. J. Levy, R. Q. Cracco, A. T. Barker, and J. C. Rothwell, "Magnetic motor stimulation: Basic principles and clinical experience," *Electroenceph. Clin. Neurophysiol.*, no. Suppl. 43, 1991.

[16] V. W. Lin, V. Wolfe, F. S. Frost, and I. Perkash, "Micturition by functional magnetic stimulation," *J. Spinal Cord Med.*, vol. 20, pp. 218–226, 1997.

[17] M. D. Craggs, M. K. M. Sheriff, J. C. Goldstone, R. Fox, and F. Middleton, "Functional magnetic stimulation (FMS) of the phrenic nerve," *Electroenceph. Clin. Neurophysiol.*, vol. 95, pp. 99P–100P, 1995.

[18] M. K. Sheriff, P. J. Shah, C. Fowler, A. R. Mundy, and M. D. Craggs, "Neuromodulation of detrusor hyper-reflexia by functional magnetic stimulation of the sacral roots," *Br. J. Urol.*, vol. 78, pp. 39–46, 1996.

[19] B.J. Roth, S. Momen, and R. Turner, "An algorithm for the design of magnetic stimulation coils," *Med. Biol. Eng. Comput.*, vol. 32, pp. 214–216, 1994.

[20] K. P. Esselle and M. A. Stuchly, "Cylindrical tissue model for magnetic field stimulation of neurons: Effects of coil geometry," *IEEE Trans. Biomed. Eng.*, vol. 42, pp. 934–941, Sept 1995.

[21] J. Ruohonen, P. Ravazzani, J. Nilsson, M. Panizza, F. Grandori, and G. Tognola, "A volume-conduction analysis of magnetic stimulation of peripheral nerves," *IEEE Trans. Biomed. Eng.*, vol. 43, pp. 669–678, July 1996.

[22] P. Ravazzani, J. Ruohonen, F. Grandori, and G. Tognola, "Magnetic stimulation of the nervous system: Induced electric field in unbounded, semi-infinite, spherical, and cylindrical media," *Ann. Biomed. Eng.*, vol. 24, pp. 606–616, 1996.

[23] A. Press, "Resistance and reactance of massed rectangular conductors," *Phys. Rev.*, vol. VIII, no. 4, pp. 417–417.

Paolo Ravazzani received the Ph.D. degree in biomedical engineering from the Polytechnic of Milan, Milan, Italy, in 1996.

He is a Researcher with the Center of Biomedical Engineering of the Italian National Research Council, Milan, Italy. His research interests concerns the study of the biological effects of electromagnetic fields, the study and modeling of magnetic stimulation of the nervous system, and biomedical signal processing.

Jarmo Ruohonen was born in 1968 in Tuupovaara, Finland. He received the M.Sc. and Ph.D. degrees in engineering physics from the Helsinki University of Technology, Helsinki, Finland, in 1993 and 1998, respectively.

From 1993 to 1997, he worked for part of the year at the Centre of Biomedical Engineering of the Italian National Research Council (C.N.R.), Milan. In 1994, he joined the BioMag Laboratory of the Helsinki University Central Hospital where he worked as the Project Manager of the development of stereotactic TMS imaging. From 1999 until 2001, he worked as the Product Manager for MR-Guided Procedures at Philips Medical Systems (formerly Marconi Medical Systems). Presently, he is Director of R&D at Nexstim Ltd., Helsinki, Finland. His research interests include EEG and TMS.

Gabriella Tognola received the Ph.D. degree in biomedical engineering from the Polytechnic of Milan, Milan, Italy, in 1999.

She is a Researcher of the Centre of Biomedical Engineering of Italian National Research Council, Milan, Italy. Her primary research interests are in magnetic stimulation, techniques of signal processing for biomedical signals, analysis and modeling of auditory functions, otoacoustic emissions, speech, and computer graphics. Her list of publications includes about 30 peer-reviewed journal, one special issue of a peer-reviewed journal (guest editor), and four chapters in international books. She has made more than 60 contributions to conferences proceedings inherent to the her research interests.

Federica Anfosso, photograph and biography not available at time of publication.

Marko Ollikainen was born in Helsinki, Finland, on 20 November, 1969. He received the M.Sc. degree in electrical engineering from the Helsinki University of Technology, Helsinki, Finland, in 1997.

In 1996, he joined the BioMag Laboratory of the Helsinki University Central Hospital as an Electrical Engineer. Since 2000, he is Development Manager for Electrical Engineering at Nexstim Ltd., Helsinki, Finland. His research interests are stereotactic magnetic stimulation of the human brain, power electronics needed in magnetic stimulation, and data acquisition and instrumentation for TMS-compatible EEG and EMG.

Risto J. Ilmoniemi was born in 1954, received M.Sc. and Ph.D. degrees in physics from the Helsinki University of Technology (HUT), Helsinki, Finland, in 1981 and 1985, respectively.

He developed biomagnetic theory and technology in the Low Temperature Laboratory of HUT from 1978 to 1993 and at New York University, New York, from 1985 to 1993. In 1992, he was appointed Docent of Neurophysics at HUT. He is currently Head of the BioMag Laboratory at the Helsinki University Central Hospital. He is also founder and Chairman of the Board of Nexstim Ltd., a company developing TMS imaging systems. His research interests include multichannel magnetometers and electrode arrays, the biomagnetic inverse problem, evoked magnetic fields, spontaneous brain activity, and transcranial magnetic stimulation.

Ferdinando Grandori is Director of the Centre of Biomedical Engineering (Italian National Research Council), Milan, Italy. His research interests are focused on the electric and magnetic stimulation of the nervous system, otoacoustic emissions, methods of response analysis and interpretation, and in the area of newborn hearing screening. He is the author of more than 60 journal articles, books, book chapters, and proceedings, and served as guest editor ditor of a number of special issues of journals.